Hamiltonian Triplet Interactions: Areal and Perimetric Forces

James D. Meiss *

Abstract.

Gravitational and electromagnetic interactions are Hamiltonian systems with forces between pairs of particles. We propose an alternative: Hamiltonian dynamics with triplet interactions between point particles. Our system has a potential energy that depends on the shape of the triangle for each triplet. Similar multi-body forces occur in many physical systems, e.g., polarizable molecules, nucleon interactions, and colloids, but typically are combined with more conventional two-body forces. We focus on potentials that depend only on the triangle perimeter or on its area. The resulting forces point towards a center of the triangle, either the incenter or the orthocenter, respectively. For the planar case, the resulting system has six degrees of freedom but can be reduced to three since it conserves the total momentum and angular momentum. The dynamics often exhibits chaotic motion, but there are a number of special solutions, for example equilateral and isosceles triangles, and perturbations of these can lie on invariant tori. Numerical investigations of several examples show families of such regular trajectories as well as examples of chaotic dynamics.

Key words. Hamiltonian chaos, multibody forces, triangular potential

MSC codes. 37J99, 37N05, 70F07, 70H07

1. Introduction: Triplet Interactions.

A classic dynamical system corresponds to a set of particles with positions and momenta $(r_i, p_i) \in \mathbb{R}^3 \times \mathbb{R}^3$ and masses m_i, where $i = 1, 2, \ldots n$. Its dynamics is obtained from a Hamiltonian $H(r,p) : \mathbb{R}^{3n} \times \mathbb{R}^{3n} \to \mathbb{R}$ that has the standard kinetic plus potential form:

$$H(r,p) = K(p) + V(r) = \sum_{i=1}^{n} \frac{\|p_i\|^2}{2m_i} + V(r) \ . \tag{1.1}$$

For standard models, such as gravitational or electrostatic interactions, the particles interact pairwise with a central force so that

$$V(r) = \sum_{j<i} U_2(r_{ij}) \ , \tag{1.2}$$

where

$$r_{ij} \equiv r_i - r_j \ .$$

The pair potential, U_2, can also depend on parameters, such as charge and mass, associated with each particle. Of course this is the case for gravitational and electrostatic interactions, (1.2).

Instead of a potential of the form (1.2), we will consider cases where the interactions correspond to a force among triplets:

Triplet Interactions. *A triplet interaction term is a function $U_3 := \mathbb{R}^3 \times \mathbb{R}^3 \times \mathbb{R}^3 \to \mathbb{R}$, that **cannot** be written as a sum of pair interactions (e.g., is unlike the potential in (1.2)).*

For this paper, we will assume the potential in (1.1) satisfies three hypotheses:

*Department of Applied Mathematics, University of Colorado, Boulder, CO 80309-0526 (James.Meiss@colorado.edu)

Hypothesis 1 (Triplet Potential). *The potential is a sum of triple interaction terms:*

$$V(r) = \sum_{i<j<k} U_3(r_i, r_j, r_k) \ .$$

In addition we will assume:

Hypothesis 2 (Central Forces). *The potential energy, $V(r)$, depends only on pairwise distances, $\|r_{ij}\|$, $i, j = 1 \dots n$, $i \neq j$.*

Of course, the gravitational potential satisfies this hypothesis. Potentials that satisfy Hyps. 1-2, depend only on the lengths of the sides of the triangle formed by each triplet of particles at positions (r_i, r_j, r_k) in $\mathbb{R}^3$, thus

$$V(r) = \sum_{i<j<k} U_\Delta(\|r_{ij}\|, \|r_{jk}\|, \|r_{ki}\|) \ . \tag{1.3}$$

For example if there are three bodies with positions $(r_1, r_2, r_3) = (u, v, w)$, and

$$a = \|w - v\|, \quad b = \|u - w\|, \text{ and } c = \|v - u\| \ , \tag{1.4}$$

(see e.g., Fig. 1) then (1.3) becomes

$$V(u, v, w) = U_\Delta(a, b, c) \ , \tag{1.5}$$

so that U_Δ is a function only of the lengths of the sides of the (u, v, w)-triangle. Of course, U_Δ could also depend on parameters, such as masses or charges.

Perhaps the simplest potential satisfying Hyp. 2 is that for harmonic springs: $U_\Delta(a, b, c) = \frac{1}{2}\left(k_1 a^2 + k_2 b^2 + k_3 c^2\right)$. However, this potential as well as those for gravitational or electrostatic forces do not satisfy Hyp. 1, since they are sums of pairwise interactions.

To make the triangular nature of the interactions more explicit, we assume:

Hypothesis 3 (Symmetry). *The potential $U_\Delta : \mathbb{R}^{3+} \to \mathbb{R}$ is permutation symmetric under particle exchange:*

$$U_\Delta(a.b.c) = U_\Delta(b, c, a) = U_\Delta(b, a, c) \ . \tag{1.6}$$

For example, note that if the masses were all equal, a gravitational potential would satisfy Hyp. 3; however, it would not satisfy Hyp. 1.

Potentials satisfying Hyps. 1-3 have been studied in the context of a number of applications, including polarizable molecules, colloids, Bose-Einstein condensates, and nucleon interactions, as we recall in §2.

In this paper we will study in detail only the simplest case: a single triplet with positions (u, v, w) and conjugate momenta (p_u, p_v, p_w). The Hamiltonian (1.1) with a potential satisfying Hyps. 1-3 then becomes

$$H(r, p) = \frac{\|p_u\|^2}{2m_u} + \frac{\|p_v\|^2}{2m_v} + \frac{\|p_w\|^2}{2m_w} + \ U_\Delta(\|v - w\|, \|w - u\|, \|u - v\|) \ . \tag{1.7}$$

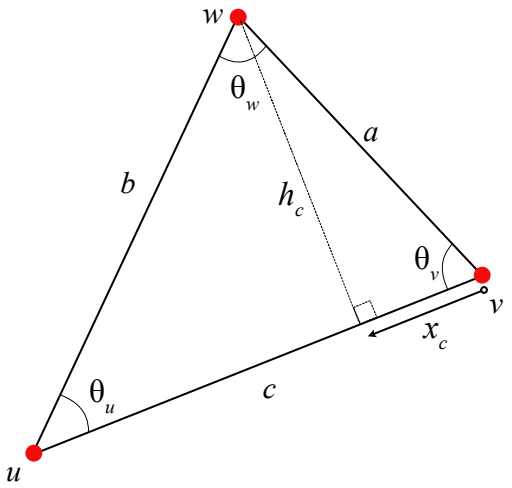

Figure 1. *A triangle with vertices u, v, w, sides a, b, c, and interior angles $\theta_u, \theta_v, \theta_w$. The altitude from side c has length h_c (A.1), and x_c (A.2) denotes the distance from v to the intersection of this altitude with side c.*

This gives the dynamics

$$\begin{aligned} \dot{p}_u &= -\partial_u U_\Delta = -\frac{u-w}{\|u-w\|}\partial_2 U_\Delta - \frac{u-v}{\|u-v\|}\partial_3 U_\Delta \\ \dot{u} &= \frac{p_u}{m_u} \ , \end{aligned} \tag{1.8}$$

with cyclic permutations for the other particles. We will rewrite these equations for specific potentials in §3, and in Jacobi coordinates in §4.

The Hamiltonian system (1.7) with three particles in $\mathbb{R}^3$ has nine degrees of freedom. Of course since the potential (1.5) has translation symmetry, $V(u+\alpha, v+\alpha, w+\alpha) = V(u,v,w)$, $\forall \alpha \in \mathbb{R}^3$, the total momentum,

$$p_T = p_u + p_v + p_w \ , \tag{1.9}$$

is conserved, and this can be used to eliminate three degrees of freedom by going to center-of-mass coordinates, i.e., translating variables by

$$R = \frac{1}{m_T}(m_1 u + m_2 v + m_3 w) \ . \tag{1.10}$$

In addition, since (1.5) has rotation symmetry: $V(Qu, Qv, Qw) = V(u,v,w)$ for any rotation matrix $Q \in SO(3)$, the total angular momentum,

$$J_T = u \times p_u + v \times p_v + w \times p_w \ , \tag{1.11}$$

is also conserved. It is also useful to note that the moment of inertia relative to the center of mass,

$$I = \sum_{i=1}^{3} m_i \|r_i - R\|^2 = \frac{1}{m_T}(m_2 m_3 a^2 + m_1 m_3 b^2 + m_1 m_2 c^2) \ , \tag{1.12}$$

is also a function only of the triangle sides.

Note that the forces in (1.8) lie in the plane of the triangle formed by (u, v, w). Thus if the initial momenta are in this plane, the orbits remain in the plane. For the planar case, we start with 3×2 degrees of freedom, and eliminate two by going to center-of-mass coordinates and one more for the angular momentum, as it is orthogonal to this plane. The resulting dynamical system has three degrees of freedom, and this can be made explicit using Jacobi coordinates, see §4.

Thus the dynamics of this simplest three-body case, unlike the simplest two-body case—the Kepler problem, is non-trivial. We will show results of numerical simulations in §5.

2. Multi-Body Forces in Applications. Multi-body interactions have been considered for a number of different physical systems. Often these are obtained as "effective interactions" between structured components such as molecules or lattices. One example is for interactions between polarizable molecules [Sto13]. A model of this is the Axilrod-Teller-Muto triple-dipole interaction [AT43] (also obtained by Muto in 1943) with the potential

$$U_{ATM} = Z \sum_{i<j<k} \frac{1 + 3\cos(\theta_i)\cos(\theta_j)\cos(\theta_k)}{(\|r_{ij}\|\|r_{ik}\|\|r_{jk}\|)^3} , \tag{2.1}$$

where, for example, θ_i is the angle between the sides r_{ij} and r_{ik} of the ijk triangle. Note that the potential (2.1) is positive for equilateral and right triangles, but is negative when the particles lie on a line, so that one angle is π.

The ATM potential appears to not be of the form (1.3), since it depends on the angles. However, since the angles are determined by the sides, as we recall explicitly in (A.3) in App. A, (2.1) satisfies Hyps. 1-3.

Examples of interactions between micro-clusters were studied in [HW80, Oks82] using a potential of the form $V = U_{LJ} + U_{ATM}$, with the Lennard-Jones two-body potential

$$U_{LJ} = \sum_{i<j} \left[\frac{1}{\|r_{ij}\|^{12}} - \frac{1}{\|r_{ij}\|^6} \right] , \tag{2.2}$$

representing the Van der Waals forces. Combining (2.2) and (2.1) gives the "LJAT" interaction. Minimum energy configurations for $3-6$ bodies as a function of the triplet strength Z were studied in [HW80]; for example, when Z is small the equilateral triangle has minimum energy, but above a critical value, the linear configuration has smaller energy. The paper [Oks82] studies the stability of the icosahedral equilibrium, which is stable at $Z = 0$. The dynamics of this model is shown to be chaotic for a single "trimer" in [CHLW97, YE97]. The LJAT model is also discussed in the book by Stone [Sto13].

Another example corresponds to the interactions of polar molecules in an optical lattice [BMZ07]; in this case there are two-body interactions together with a three-body potential for which one model is the Hubbard potential

$$U_H = \sum_{i<j<k} \left(\frac{1}{\|r_{ij}\|^3 \|r_{jk}\|^3} + \text{cyclic permutations} \right) .$$

An alternative form for multi-body interactions was used by Baskes [Bas99] to study crystalline lattices:

$$V = U_{LJ} + \sum_{i=1} \bar{\rho}_i (\ln(\bar{\rho}_i) - 1) ,$$

where $\bar{\rho}_i$ is a background electron density for the i^{th} particle due to its Z neighbors defined by

$$\bar{\rho}_i = \frac{1}{Z}\sum_{j\neq i} \exp(-\beta(\|r_{ij}\| - 1)) \ .$$

This approach is used to study lattices, and is a version of the "Embedded Atom Method" [DFB93]. For the three body case, where $Z = 2$, the multi-body portion of this potential satisfies Hyps. 1-3. A spine fit to three-body forces was used to obtain similar potentials for a Vanadium lattice in [LS16].

Multi-body forces are also relevant in colloids, due to the nonlinearities in the Poisson-Boltzmann equations. In [RvGDvR02] the authors consider hard spheres in a salt solution and numerically compute—to lowest order in an expansion—the effects of the screening due to the fluid on the interaction between the spheres. Empirically they find that the three-body interactions closely fits a potential of the Yukawa form

$$U_Y = -\sum_{i<j<k} \frac{e^{-\gamma(\|r_{ij}\|+\|r_{jk}\|+\|r_{ki}\|)}}{\|r_{ij}\| + \|r_{jk}\| + \|r_{ki}\|} \ , \tag{2.3}$$

so that it depends only upon the perimeter of each triangle. For this system, there is also a two-body, repulsive, Yukawa potential. In §3.1, we consider similar potentials that depend only upon the perimeter.

Other examples of multi-body forces include the quantum physics of BECs [Kö02, JTPW09]. where the potential depends only upon inter-particle distances. Three-nucleon forces are also important for nuclear stability [FDGG24], describe interactions with mesons and pions [SS60, Ham15, CPW83] and arise in "chiral effective field theory" [Heb21].

In the context of non-Hamiltonian and dissipative systems, multi-particle forces have been used in generalizations of the Kuramoto model often used to study synchronization in networks of coupled oscillators, see e.g., [Str00]. Multi-particle interactions correspond, in this case, to interactions on hyper-graphs or simplicial complexes [LR20, ZLB23]. For example, [Loh22] considered multi-body interactions between higher-dimensional phase oscillators. This non-Hamiltonian system has oscillators with positions $r_i \in \mathbb{S}^2 = \{r \in \mathbb{R}^3 : \|r\| = 1\}$ and frequencies ω_i. For triplet interactions, Lohr uses the potential

$$U_L = \sum_{i,j,k} \varepsilon_{ijk} r_i \cdot r_j \times r_k \ ,$$

where ε_{ijk} is the completely antisymmetric Levi-Civita symbol. Upon adding the constraint, using Lagrange multipliers, that the particles remain on the sphere, the dissipative dynamics become

$$\dot{r_i} = \omega_i \times r_i + \frac{\lambda}{N^2}\sum_{j,k=1}^{N} \varepsilon_{ijk}[r_j \times r_k - r_i(r_i \cdot r_j \times r_k)] \ .$$

Similar models are also studied in [DKM+21], but with a symmetric coupling, giving equations of the form

$$\dot{r_i} = \omega_i \times r_i + \frac{\lambda}{N^2}\sum_{j,k=1}^{N} r_j \cdot r_i(r_k - (r_k \cdot r_i)r_i) \ ,$$

as well as higher dimensional cases. These interactions do not satisfy Hyp. 2.

In [KPS22] the gradient flow with a potential that depends upon the volume of a simplex is considered. For example, for triplet interactions they use

$$U_\Delta = \frac{\kappa_2}{6N^2} \sum_{i,j,k=1}^{N} \|A(r_i, r_j, r_k)\|^2 \,,$$

where $A(u, v, w)$ is the (vector) area of the triangle with vertices u, w, w (see (3.4)). Using Heron's formula (A.4) for the area (see App. A), the resulting equations become

$$\dot r_i = \frac{\kappa_2}{8N^2} \sum_{j,k=1}^{N} \left(\|r_{jk}\|^2 (r_j + r_k - 2r_i) + (\|r_{ik}\|^2 - \|r_{ij}\|^2)(r_j - r_k) \right) \,.$$

Since this is a gradient system, the dynamics implies that areas collapse to zero, so the particles will collapse to a line. We will assume the potential is a function of the area in the Hamiltonian context in §3.2.

3. Three Body Forces. In the remainder of this paper we will treat two special cases of a three-body potential (1.5) that satisfies Hyps. 1-3. For simplicity, we assume that there are only three-body forces, neglecting the two-body terms that appear in most of the applications in §2. Denoting the positions of the three particles by $u, v, w \in \mathbb{R}^3$ and their momenta by $p_u, p_v, p_w \in \mathbb{R}^3$, gives a Hamiltonian of the form (1.7)

In §3.1, we assume that the potential, U_Δ, is a function only of the triangle's perimeter, and in §3.2, only of its area.

3.1. Perimetric Forces. Suppose first that $U_\Delta = U(P)$, depends only on the *perimeter* of the triangle (recall (2.3)),

$$P(u, v, w) = \|w - v\| + \|u - w\| + \|v - u\| = a + b + c \,, \tag{3.1}$$

where a, b, c are the side lengths seen in Fig. 1. In the simplest case $U(P) = P$; however, this does not satisfy Hyp. 1 since it is a sum of pair interactions. We considered several cases, but concentrate on the simplest, $U(P) = \frac{1}{2}P^2$.

The resulting equations of motion (1.8) become

$$\begin{aligned} \dot p_u &= U'(P) \left(\frac{v - u}{c} + \frac{w - u}{b} \right) \,, \\ \dot u &= \frac{p_u}{m_u} \,, \end{aligned} \tag{3.2}$$

with cyclic permutations for the other two particles.

Note that the force vectors in (3.2) bisect the interior angles of the triangle, pointing into its interior if $U'(P) > 0$, see Fig. 2. These three force vectors define lines that meet at the so-called *incenter* of the triangle,

$$c_i = \frac{au + bv + cw}{P} \,, \tag{3.3}$$

the center of the circle inscribed in the triangle, see App. C. To see this, note that the two right triangles formed from a particle's force vector with each of the triangle edges coming from that

particle are congruent: i.e., the three orange edges in Fig. 2 have equal lengths and are radii of the inscribed circle.

If the particles become collinear at any time, then the middle particle is at the incenter. Moreover, in this case the perimeter is twice the maximum distance. For example, if v is between u and w, then $a + c = b$ and $P = 2b$. In this case $c_i = v$: the incenter (3.3) is the position of the central particle.

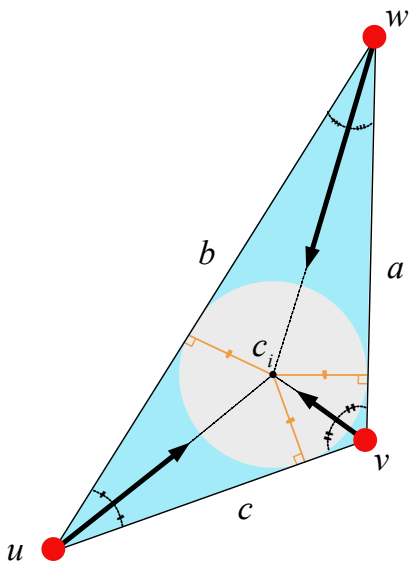

Figure 2. *Sketch of the forces acting on a triple of particles at u, v, w when the potential is a function of the perimeter of the triangle. By (3.2) force vectors bisect the angles at each vertex, and thus meet at the incenter of the triangle when $U'(P) > 0$, see App. C.*

The rate of change of the perimeter of the triangle is

$$\frac{d}{dt}P = \frac{1}{a}(v-w)\cdot(\dot{v}-\dot{w}) + \frac{1}{b}(w-u)\cdot(\dot{w}-\dot{u}) + \frac{1}{c}(u-v)\cdot(\dot{u}-\dot{v}) \ .$$

Combining this with (3.2) gives

$$\frac{d}{dt}U(P) = U'(P)\frac{d}{dt}P = -\left(\dot{u}\cdot\dot{p}_u + \dot{v}\cdot\dot{p_v} + \dot{w}\cdot\dot{p_w}\right) = -\frac{d}{dt}K \ ,$$

where K is the kinetic energy, e.g. (1.7): energy is conserved.

Using (3.3), rate of change of the incenter is

$$\frac{d}{dt}c_i = \frac{1}{P}\left(a\dot{u} + b\dot{v} + c\dot{w} + \dot{a}(u-c_i) + \dot{b}(v-c_i) + \dot{c}(w-c_i)\right) \ .$$

3.2. Areal Forces. Suppose now that U_Δ depends only on the *area* of the triangle formed by a triplet. We denote the (vector) area of a triangle by

$$\begin{aligned} A(u,v,w) &= \tfrac{1}{2}(v-u)\times(w-u) \\ &= \tfrac{1}{2}(u\times v + v\times w + w\times u) \ . \end{aligned} \tag{3.4}$$

This vector is normal to the face of the triangle; in 2D $A = \hat{e}_3 \|A(u,v,w)\|$ when u, v, w are a right-handed triplet. The form (3.4) is invariant under even permutations of the vertices, and its magnitude is permutation invariant:

$$\|A(u,v,w)\| = \|A(v,u,w)\| = \|A(w,v,u)\| \ .$$

Moreover, the area is a function only of the lengths of the sides of the triangle, as can be seen most explicitly in Heron's formula (A.4) in App. A. Thus a potential that depends only upon $\|A\|$ obeys Hyps. 1-3.

The resulting equations of motion for the Hamiltonian (1.7) become

$$\begin{aligned} \dot{p}_u &= -U'(\|A\|)\frac{1}{2\|A\|}\nabla_u \|A\|^2, \\ \dot{u} &= \frac{p_u}{m_u}, \end{aligned}$$

with cyclic permutations. Using the summation convention and (3.4), the derivative of the squared area with respect to a component of u becomes

$$\begin{aligned} \frac{\partial}{\partial u_\alpha}\|A\|^2 = 2A_i\frac{\partial A_i}{\partial u_\alpha} &= \tfrac{1}{2}\varepsilon_{ijk}(w_j - v_j)(u_k - v_k)\varepsilon_{i\beta\alpha}(w_\beta - v_\beta) \\ &= \tfrac{1}{2}\left[(w_\beta - v_\beta)(u_\alpha - v_\alpha)(w_\beta - v_\beta) - (w_\alpha - v_\alpha)(u_\beta - v_\beta)(w_\beta - v_\beta)\right] \\ &= \tfrac{1}{2}\left[(u_\alpha - v_\alpha)\|w - v\|^2 - (w_\alpha - v_\alpha)(u - v)\cdot(w - v)\right]. \end{aligned}$$

Thus in vector notation

$$\begin{aligned} \nabla_u\|A\|^2 &= \tfrac{1}{2}[(u - v)\|w - v\|^2 - (w - v)((u - v)\cdot(w - v))] \\ &= \tfrac{1}{2}(w - v)\times[(u - v)\times(w - v)] \\ &= (v - w)\times A \ . \end{aligned}$$

This vector is orthogonal to both the opposite side vector $v - w$ and to A:

$$(v - w)\cdot\nabla_u\|A\|^2 = A\cdot\nabla_u\|A\|^2 = 0 \ .$$

Consequently, the equations of motion become

$$\begin{aligned} \dot{p}_u &= m_1\ddot{u} = -\tfrac{1}{2}U'(\|A\|)(v - w)\times\hat{A} \ , \\ \dot{p}_v &= m_2\ddot{v} = -\tfrac{1}{2}U'(\|A\|)(w - u)\times\hat{A} \ , \\ \dot{p}_w &= m_3\ddot{w} = -\tfrac{1}{2}U'(\|A\|)(u - v)\times\hat{A} \ , \end{aligned} \tag{3.5}$$

where $\hat{A} = A/\|A\|$ is the unit vector in the direction of the area.

As sketched in Fig. 3 the resulting force vectors in (3.5) are in the plane of the triangle and are orthogonal to the opposite side of the triangle: they are parallel to the triangle's altitudes. As recalled in App. D, the altitudes have a common intersection, the *orthocenter* of the triangle. When the triangle is acute, and $U' > 0$, the forces point inward, and the orthocenter is in the interior of the triangle. However, when the triangle has an obtuse angle, two of the force vectors point outward, and the orthocenter is exterior to the triangle.

Naturally, these equations also preserve the total momentum (1.9) and total angular momentum (1.11). Note that the rate of change of the area of the triangle is

$$\frac{d}{dt}A(u,v,w) = \tfrac{1}{2}\left(\dot{u}\times(v - w) + \dot{v}\times(w - u) + \dot{w}\times(u - v)\right).$$

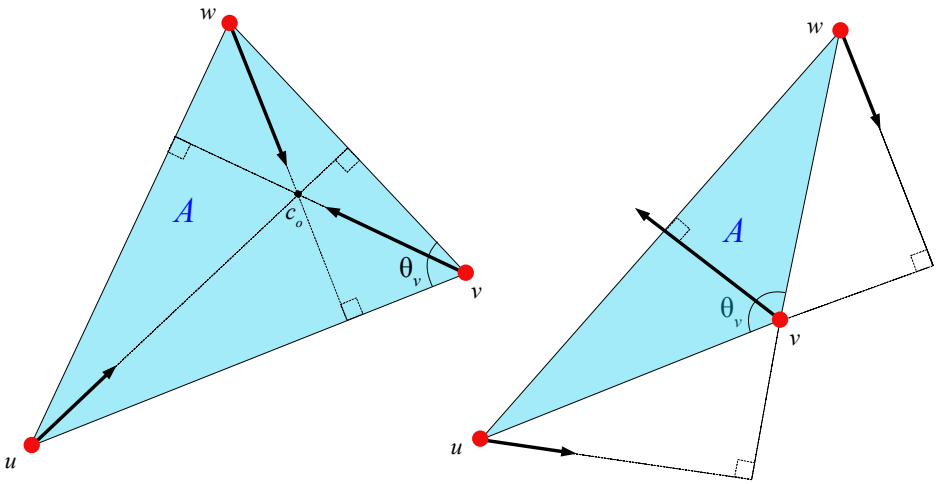

Figure 3. *Sketches of the forces acting on a triplet of particles at u, v, w when the potential is a function of the area. The forces are orthogonal to the opposite sides and meet at the orthocenter, c_o.*

3.3. Special Solutions. There are a number of special configurations for which the dynamics is simpler. For simplicity we suppose that all the masses are equal

$$m_u = m_v = m_w = 1 \,, \tag{3.6}$$

the center of mass (1.10) is the origin, and the total momentum (1.9) is zero.

- (Equilateral Triangle) Suppose that the initial state has a discrete rotational symmetry:

$$\begin{aligned} v(0) &= Q_{2\pi/3} u(0) \,, \quad & w(0) &= Q_{4\pi/3} u(0) \,, \\ \dot{v}(0) &= Q_{2\pi/3} \dot{u}(0) \,, \quad & \dot{w}(0) &= Q_{4\pi/3} \dot{u}(0) \,, \end{aligned} \tag{3.7}$$

  where Q_ϕ is the 2D rotation by angle ϕ. This corresponds to an equilateral triangle with sides

$$a = b = c = \sqrt{3} \|u\| \,,$$

  so that the perimeter and area become

$$\begin{aligned} P &= 3^{3/2} \|u\| \,, \\ A &= \tfrac{3^{3/2}}{4} \|u\|^2 \,. \end{aligned}$$

  The rotational symmetry of the initial conditions is maintained by (3.2) and (3.5), so the shape remains equilateral. Letting $u = r(\cos\theta, \sin\theta)$, the system can be reduced to a Hamiltonian with coordinates (r, θ), and momenta $p_r = \dot{r}$ and $p_\theta = r^2 \dot{\theta}$:

$$H(r, \theta, p_r, p_\theta) = \tfrac{1}{2} p_r^2 + \frac{p_\theta^2}{2r^2} + \tfrac{1}{3} U \,,$$

  Note that this is an integrable system, since the angular momentum is conserved. Assuming that U is monotonically increasing, the uniformly rotating case corresponds to $p_\theta^2 = \sqrt{3} U'(P) r^3$ or $\frac{1}{2\sqrt{3}} U'(A) r^4$, for the perimetric and areal cases, respectively.

- (Isosceles) For an isosceles triangle with base b and height h, we can set $u(t) = (-b/2, -h/3)$, $v(t) = (0, 2h/3)$ and $w(t) = (b/2, -h/3)$. This form is a solution of (3.2) and (3.5) maintaining the symmetry. Here

$$P(t) = |b| + \sqrt{b^2 + 4h^2}\ ,$$
$$A(t) = -\tfrac{1}{2} bh\hat{z}\ .$$

  Note that the area is negative for our assumed coordinates when $bh > 0$ since the orientation of the triangle is reversed. The dynamics can be reduced to a two degree of freedom Hamiltonian

$$H(b, h, p_b, p_h) = p_b^2 + \tfrac{3}{4} p_h^2 + U(b, h)\ .$$

  For the perimetric case, the equations become

$$\ddot{h} = \tfrac{3}{2}\dot{p}_h = -6U'(P)\frac{h}{\sqrt{b^2 + 4h^2}}\ ,$$
$$\ddot{b} = 2\dot{p}_b = -2U'(P)\left(\operatorname{sgn}(b) + \frac{b}{\sqrt{b^2 + 4h^2}}\right)\ .$$

  Similarly the equations for the areal case are

$$\ddot{b} = 2\dot{p}_b = -U'(\|A\|)|h|\operatorname{sgn}(b)\ ,$$
$$\ddot{h} = \tfrac{3}{2}\dot{p}_h = -\tfrac{3}{4}U'(\|A\|)|b|\operatorname{sgn}(h)\ .$$

  These equations are not smooth for a pair collision when $b = 0$, or a linear configuration when $h = 0$.
- (Rotating Line) Suppose that the particles lie on a line, and one is at the center of mass, say $v = 0$, so that $u = -w$. This linear configuration is preserved if $\dot{u}(0) = -\dot{w}(0)$ and $\dot{v} = 0$. Using polar coordinates, $u = r(\cos(\theta), \sin(\theta))$, the perimeter is $P = 4r$, and the reduced Hamiltonian for the perimetric case becomes

$$H(r, \theta, p_r, p_\theta) = \tfrac{1}{2} p_r^2 + \frac{p_\theta^2}{2r^2} + \tfrac{1}{2} U(4r)\ .$$

  Since the angular momentum is conserved, this again reduces to one degree-of-freedom. If $U(P)$ is increasing, this has the uniformly rotating solution when $p_\theta^2 = 2r^3 U'(P)$. A special case of this corresponds to zero angular momentum. Again assuming $U(P)$ is monotone increasing, this gives oscillations with repeated triple collisions.

4. Jacobi Coordinates. To explicitly eliminate the conserved quantities we can use, for example, Jacobi coordinates [MH92, LR97, LMAC98, Mon17]). For the triplet $(r_1, r_2, r_3) = (u, v, w)$, one version of these coordinates is

$$\begin{aligned} s &= v - u\ , \\ h &= w - \frac{m_1 u + m_2 v}{m_{12}} = \frac{m_1(w-u) + m_2(w-v)}{m_{12}}\ , \\ R &= \frac{1}{m_T}(m_1 u + m_2 v + m_3 w)\ , \end{aligned} \tag{4.1}$$

where $m_T = m_1 + m_2 + m_3$ and $m_{12} = m_1 + m_2$. As sketched in Fig. 4, the vector s is one side of the triangle, h is the vector from the center-of-mass of u and v to the vertex w, and R is the center-of-mass of the triplet. The inverse of (4.1) is

$$\begin{aligned} u &= R - \frac{m_2}{m_{12}} s - \frac{m_3}{m_T} h \,, \\ v &= R + \frac{m_1}{m_{12}} s - \frac{m_3}{m_T} h \,, \\ w &= R + \frac{m_{12}}{m_T} h \,. \end{aligned} \tag{4.2}$$

The main points of the choice (4.1) are: (i) this linear transformation is orthogonal with respect to the mass-scaled metric, so the kinetic energy remains diagonal, and (ii) (s, h) are invariant under translations, $(u, v, w) \to (u, v, w) + (\alpha, \alpha, \alpha)$ [Mon17]. Indeed the kinetic energy becomes

$$K = \tfrac{1}{2} \left(\mu_1 \|\dot{s}\|^2 + \mu_2 \|\dot{h}\|^2 + m_T \|\dot{R}\|^2 \right) \,, \tag{4.3}$$

where

$$\frac{1}{\mu_1} \equiv \frac{1}{m_1} + \frac{1}{m_2}, \quad \frac{1}{\mu_2} \equiv \frac{1}{m_{12}} + \frac{1}{m_3} \,,$$

define the "reduced masses". Since by Hyp. 2, the potential is independent of the center-of-mass R, the momentum $p_R = m_T \dot{R}$ is conserved, and we can drop it from the Hamiltonian so that

$$H = \tfrac{1}{2\mu_1} \|p_s\|^2 + \tfrac{1}{2\mu_2} \|p_h\|^2 + U(s, h) \,. \tag{4.4}$$

For the planar case, this is a four degree-of-freedom system. The angular momentum (1.11) becomes

$$J_T = s \times p_s + h \times p_h \,,$$

which of course is conserved. Similarly the moment of inertia in center-of-mass coordinates (1.12) becomes, in Jacobi coordinates,

$$I = \mu_1 \|s\|^2 + \mu_2 \|h\|^2 \,. \tag{4.5}$$

In Jacobi coordinates, the perimeter (3.1) becomes

$$P = a + b + c = \frac{1}{m_{12}} \left(\|m_1 s - m_{12} h\| + \|m_2 s + m_{12} h\| \right) + \|s\| \,.$$

When the potential depends only on P, the Hamiltonian equations for (4.4) are

$$\begin{aligned} \dot{p}_s &= -U'(P) \left(\frac{s}{\|s\|} + \frac{m_1}{m_{12}} \frac{m_1 s - m_{12} h}{\|m_1 s - m_{12} h\|} + \frac{m_2}{m_{12}} \frac{m_2 s + m_{12} h}{\|m_2 s + m_{12} h\|} \right) , \\ \dot{p}_h &= -U'(P) \left(\frac{m_{12} h - m_1 s}{\|m_{12} h - m_1 s\|} + \frac{m_{12} h + m_2 s}{\|m_{12} h + m_2 s\|} \right) , \\ \dot{s} &= \tfrac{1}{\mu_1} p_s, \\ \dot{h} &= \tfrac{1}{\mu_2} p_h. \end{aligned} \tag{4.6}$$

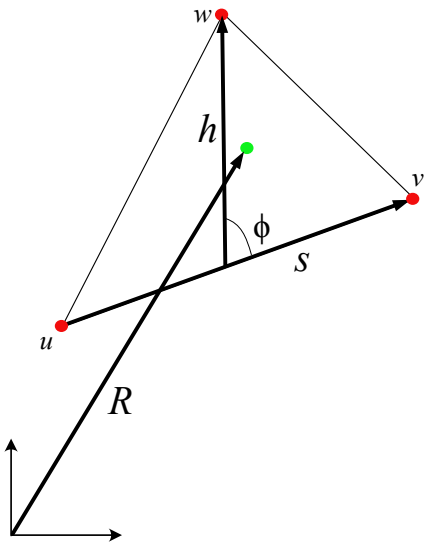

Figure 4. *Jacobi coordinates (s, h, R) for the triangle.*

For the areal case, since $v - u = s$ and $w - u = h + \frac{m_2}{m_{12}} s$, the area (3.4) becomes

$$A(u, v, w) = \tfrac{1}{2} s \times (h + \tfrac{m_2}{m_{12}} s) = \tfrac{1}{2} s \times h,$$

which is natural since s is a side and h is a vector connecting that side to the third vertex. When the potential is a function of area, the equations for (4.4) are

$$\begin{aligned} \dot{p}_s &= -\tfrac{1}{2} U'(\|A\|) h \times \hat{A} \,, \\ \dot{p}_h &= -\tfrac{1}{2} U'(\|A\|) \hat{A} \times s \,, \\ \dot{s} &= \tfrac{1}{\mu_1} p_s \,, \\ \dot{h} &= \tfrac{1}{\mu_2} p_h \,. \end{aligned} \tag{4.7}$$

To eliminate the angular momentum we introduce polar coordinates following [Mon17]. Using complex notation, $\mathbb{R}^2 \simeq \mathbb{C}$, let

$$s = \sigma e^{i\theta} \,, \quad h = \eta e^{i(\theta+\phi)} \,.$$

Substituting into (4.3) gives the kinetic energy

$$K = \tfrac{1}{2} \left(\mu_1 \dot{\sigma}^2 + \mu_2 \dot{\eta}^2 + \mu_1 \sigma^2 \dot{\theta}^2 + \mu_2 \eta^2 (\dot{\theta} + \dot{\phi})^2 \right) \,.$$

The Lagrangian $L = K - V$ does not depend upon the rotation angle θ: the shape of the triangle is determined by (σ, η, ϕ). This will give the conserved angular momentum, $p_\theta = J_T$,

$$p_\theta = \frac{\partial L}{\partial \dot{\theta}} = \mu_1 \sigma^2 \dot{\theta} + \mu_2 \eta^2 (\dot{\theta} + \dot{\phi}) \,.$$

Since (4.5) gives $I = \mu_1 \sigma^2 + \mu_2 \eta^2$, eliminating $\dot{\theta}$ in the kinetic energy gives

$$K = \tfrac{1}{2} \left(\mu_1 \dot{\sigma}^2 + \mu_2 \dot{\eta}^2 + \frac{p_\theta^2}{I} + \frac{\mu_1 \mu_2 \sigma^2 \eta^2}{I} \dot{\phi}^2 \right) \,.$$

Defining canonical momenta,

$$p_\sigma = \mu_1 \dot{\sigma}, \quad p_\eta = \mu_2 \dot{\eta}, \quad p_\phi = \frac{\mu_1 \mu_2 \sigma^2 \eta^2}{I} \dot{\phi} \ ,$$

then gives

$$H = \frac{p_\sigma^2}{2\mu_1} + \frac{p_\eta^2}{2\mu_2} + \frac{p_\theta^2}{2I} + \frac{1}{2}\left(\frac{1}{\mu_1 \sigma^2} + \frac{1}{\mu_2 \eta^2}\right) p_\phi^2 + U(\sigma, \eta, \phi) \ . \tag{4.8}$$

The potential is a function only of the lengths σ, η and the angle ϕ; therefore, this is a three degree-of-freedom system for $(\sigma, p_\sigma), (\eta, p_\eta)$, and (ϕ, p_ϕ).

The perimeter and area become

$$\begin{aligned} P &= \frac{1}{m_{12}}(|m_{12}\eta e^{i\phi} - m_1 \sigma| + |m_{12}\eta e^{i\phi} + m_2 \sigma|) + \sigma \ , \\ A &= \tfrac{1}{2}\sigma\eta \sin(\phi) \ . \end{aligned}$$

The configuration equations for (4.8) become

$$\begin{aligned} \dot{\sigma} &= \frac{1}{\mu_1} p_\sigma \ , \\ \dot{\eta} &= \frac{1}{\mu_2} p_\eta \ , \\ \dot{\phi} &= \left(\frac{1}{\mu_1 \sigma^2} + \frac{1}{\mu_2 \eta^2}\right) p_\phi \ , \end{aligned} \tag{4.9}$$

and for areal potentials the momentum equations are

$$\begin{aligned} \dot{p_\sigma} &= \mu_1 \frac{p_\theta^2}{I^2}\sigma + \frac{p_\phi^2}{\mu_1 \sigma^3} - \tfrac{1}{2}U'(\|A\|)\eta |\sin(\phi)| \ , \\ \dot{p_\eta} &= \mu_2 \frac{p_\theta^2}{I^2}\eta + \frac{p_\phi^2}{\mu_2 \eta^3} - \tfrac{1}{2}U'(\|A\|)\sigma |\sin(\phi)| \ , \\ \dot{p_\phi} &= -\tfrac{1}{2}U'(\|A\|)\sigma\eta \cos(\phi)\, \mathrm{sign}(\sin(\phi)) \ . \end{aligned} \tag{4.10}$$

The corresponding equations for the perimetric case are complicated, and we do not write them out.

5. Numerical Explorations. A typical trajectory of the three body system (1.7) with $m_1 = m_2 = m_3 = 1$ and $U(P) = \frac{1}{2}P^2$ is shown in Fig. 5. In panel (a), the particle positions are shown in the (x, y) plane. The initial conditions are indicated by filled circles, and curves for the three particles, red for u, green for v and blue for w, show the trajectories up to $t = 20$. The integration was done using the *RK45* method in Matlab, with an error bound of 10^{-12}. As one estimate of the integration accuracy, the energy and angular momentum have errors $\mathcal{O}(5 \times 10^{-10})$ over an integration time of $t = 500$. Panel (b) shows the same trajectory in the 3D space of inequities (i_a, i_b, i_c) (see App. B). We claim these coordinates are more convenient than the three side lengths, (a, b, c), since the triangle inequalities restrict the latter to a hard-to-visualize cone in the positive octant, while the inequities can take any values in the non-negative octant.

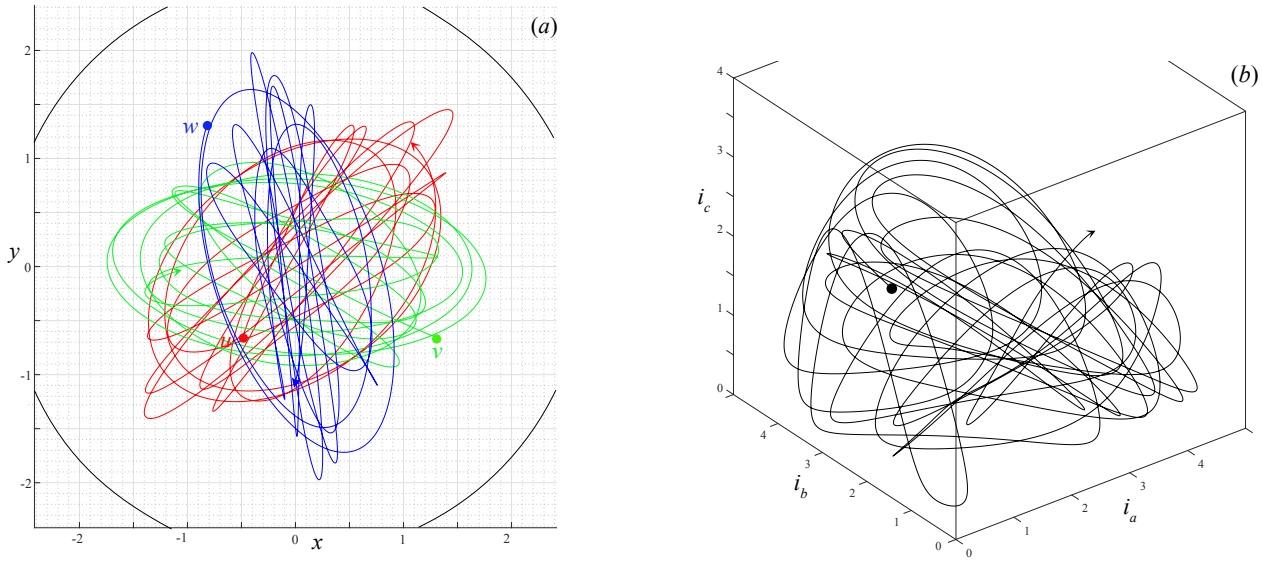

Figure 5. *(a) Positions of the three particles (u, v, w) in the plane as a function of time, up to $t = 20$ for $U(P) = \frac{1}{2}P^2$. (b) Trajectory in the positive octant of the inequities, (i_a, i_b, i_c), see App. B. At $t = 0$, the triangle has sides $(a, b, c) = (2.9, 2.0, 1.8)$. With the center-of-mass at the origin this gives $u_0 \simeq (-0.49166 - 0.65781)$, $v_0 \simeq (1.30833, -0.65781)$, and $w_0 \simeq (-0.81666, 1.31561)$, The initial velocities are $\dot{u} = -\dot{w} = (1, 3)$ and $\dot{v} = 0$. For this trajectory $E = 32.445$ and $J_T = 2.94842$.*

If one plots longer segments of this trajectory, one gets the impression it is chaotic. To see this in more detail, Fig. 6 shows $P(t)$ and $A(t)$ along this trajectory. These curves are computed using $RelTol = AbsTol = 10^{-12}$; if this is relaxed, the resulting curves for P and A appear close to those seen in the figure up to $t \approx 200$, but after that the evolution is quite different, again as one would expect for a chaotic orbit.

Note that since $E = K + U$, and the kinetic energy is non-negative, the maximal perimeter for this quadratic potential is $P \le \sqrt{2E}$. For the initial condition in Fig. 5, the energy is $E = 32.445$, implying that $P \le 8.0554$. However, for this trajectory the angular momentum (1.11) is nonzero, so the maximal perimeter is determined by

$$E = \frac{J_T^2}{2I} + U(P) \; . \tag{5.1}$$

For a given perimeter and equal unit masses, the moment of inertia (1.12) has the bound $I \ge P^2/9$, which is reached when the triangle is equilateral. Indeed, for the trajectory of Fig. 6, $I_{min} = 0.144625 > P_{min}^2/9 = 0.1439709$. Using this in (5.1) for the quadratic potential, then gives

$$P_{max} = \sqrt{E + \sqrt{E^2 - 9J_T^2}} = 7.9788 \; . \tag{5.2}$$

The maximum realized up to $t = 500$, as seen in Fig. 6(a), is 99.9% of this value.

For a given perimeter the maximum side length occurs when the triangle collapses to a line, so we must have sides of length less than $P/2$. The largest distance from the center-of-mass would occur at a double collision, where two of the particles are at a distance $P/6$ from the center-of-mass and the third is at the distance $P/3$. This gives a version of Hill's region: the trajectory must lie in the disk of radius $\frac{1}{3}P_{max} \simeq 2.6596$ about the center-of-mass; this disk is shown in Fig. 5(a).

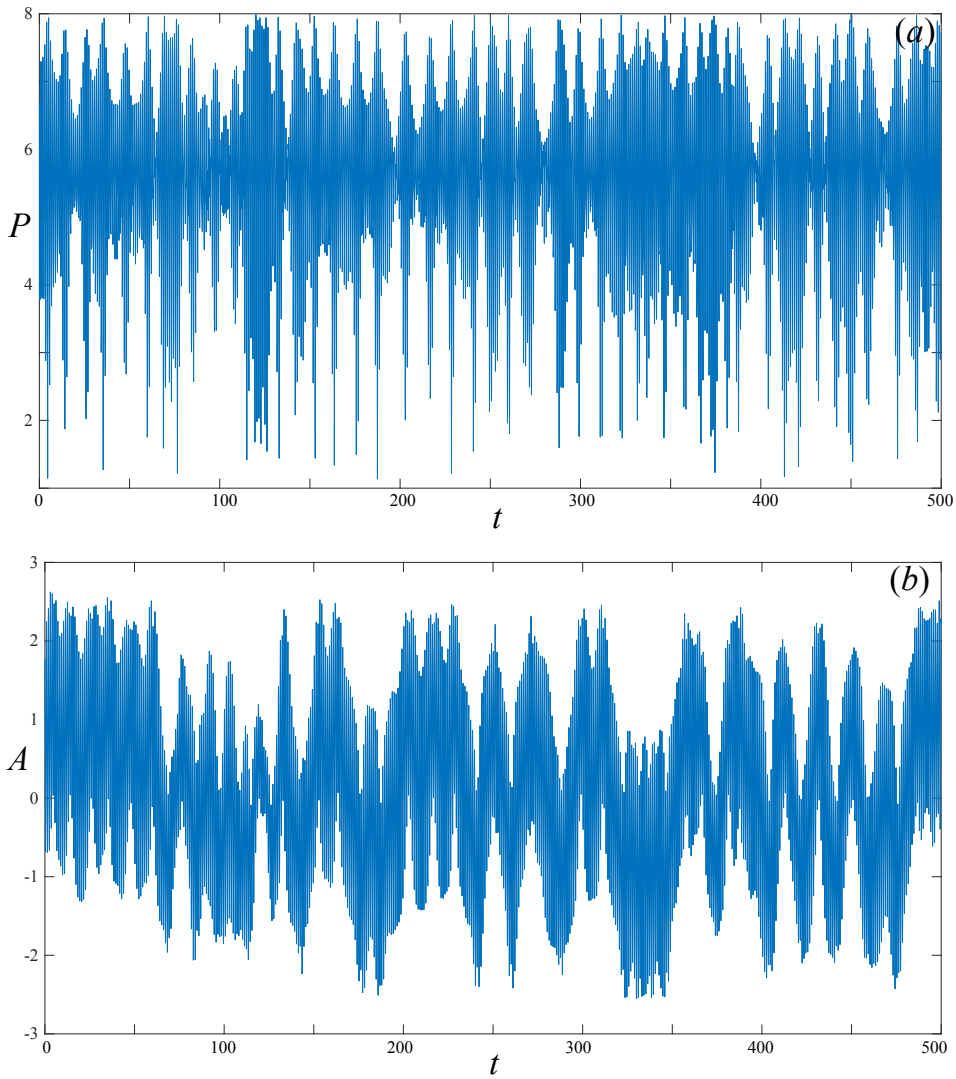

Figure 6. *For the potential* $U(P) = \frac{1}{2}P^2$ *and the initial condition of Fig. 5, the perimeter (a) and area (b) as a function of time for* $t \in [0, 500]$. *For this trajectory segment,* $P \in [1.138305, 7.985506]$, $A \in [-2.552623, 2.623263]$ *and the moment of inertia (1.12)* $I \in [0.144625, 8.125064]$.

The area along the trajectory is shown in Fig. 6(b). For this triangle, $A(0) = 1.77607$ and $A(t)$ initially decreases, crossing zero when the triangle collapses to a line and then reverses orientation. For a given perimeter the area has an upper bound given by (B.3) in App. C, corresponding to the equilateral case. Thus, since the perimeter is bounded by (5.2), $|A(t)| \leq 3.06289$. The trajectory for this example only reaches 86% of this bound over the time shown in the figure.

We computed the maximal Lyapunov exponent, μ, for this trajectory by integrating the one-jet equations (E.1). As an initial condition, we chose a random deviation vector that left the center of mass at the origin. For $T = 2000$, we found $\mu_T = 0.16905 \pm 0.00008$, where the nominal error is measured by the variation in μ_T over the interval $T \in [1600, 2000]$. As usual it is difficult to give an accurate value for μ [SM25], but at least this indicates that the trajectory is chaotic.

The variation of the maximal Lyapunov exponent with changing initial velocity is shown in Fig. 7. For this one-parameter family of trajectories, μ_{2000} appears to be positive. The three curves in this figure show the value of the exponent with different, randomly chosen, initial deviation vectors; this gives an indication of the large errors in the computation.

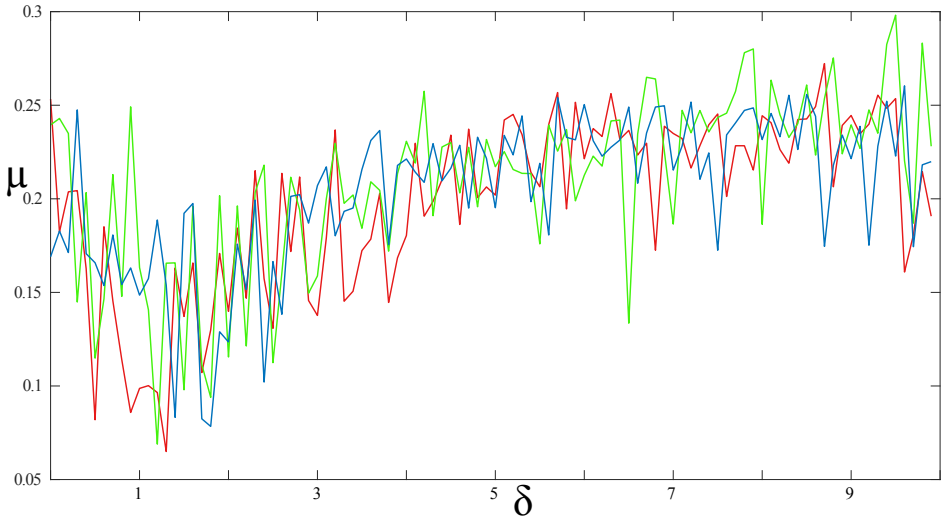

Figure 7. *Computations of the maximal Lyapunov exponent μ_T for the potential $U(P) = \frac{1}{2}P^2$ and integration time $T = 2000$. The initial condition is a triangle with sides $(a, b, c) = (2.9, 2.0, 1.8)$ and initial velocities $\dot{u} = -\dot{w} = (1+\delta, 3)$ and $\dot{v} = 0$. When $\delta = 0$, this corresponds to the case shown in Fig. 5. The three curves differ only in that different randomly chosen deviation vectors were used. Large variations show the slow convergence of the Lyapunov exponent.*

We now consider a trajectory that is close to the uniformly rotating equilateral triangle $a = b = c$ of §3.3. Such a trajectory simply rotates when the velocities have magnitude

$$V_{rot} = \sqrt{aU'(P)}\,;$$

which for the quadratic potential becomes $V_{rot} = \sqrt{3}a$. An example with the velocities perturbed is shown in Fig. 8. In this case the trajectory appears to lie on a three torus.[1] Indeed the maximal Lyapunov exponent for this case seems to be 0: $\mu_{200} = 0.013 \pm 0.008$ and $\mu_{2000} = 0.0029 \pm 0.0008$. Both the area $A \in [1.477951, 5.200333]$ and perimeter $P \in [6.984039, 11.026097]$ oscillate quasiperiodically (not shown).

The Lyapunov exponent for a range of equilateral initial conditions (those in Fig. 8 with $\delta \in [0, 10]$) is shown in Fig. 9. The estimated Lyapunov exponent appears to be essentially zero up to $\delta = 4.2$, where there is a sudden onset of chaotic behavior. The short time behavior for several of these regular orbits is shown in Fig. 10 in inequity space. The inner three orbits in the figure appear to lie on invariant tori enclosing the uniformly rotating equilateral case (the point $i_a = i_b = i_c = 2\sqrt{3}$). The outermost (gray) trajectory, with $\delta = 4.5$, is chaotic as seen in Fig. 9. A longer segment of a trajectory in this family, for $\delta = 3.0$, was shown in Fig. 8.

The $\delta = 4.5$, chaotic orbit of Fig. 10 appears to have near pair-collisions since it approaches the axes in inequity space. The first near collision is at $t = 0.498$, where $b = 0.0924$, so $u \approx w$; this is

[1] Since we have not eliminated the angular momentum here, we nominally have six degrees of freedom.

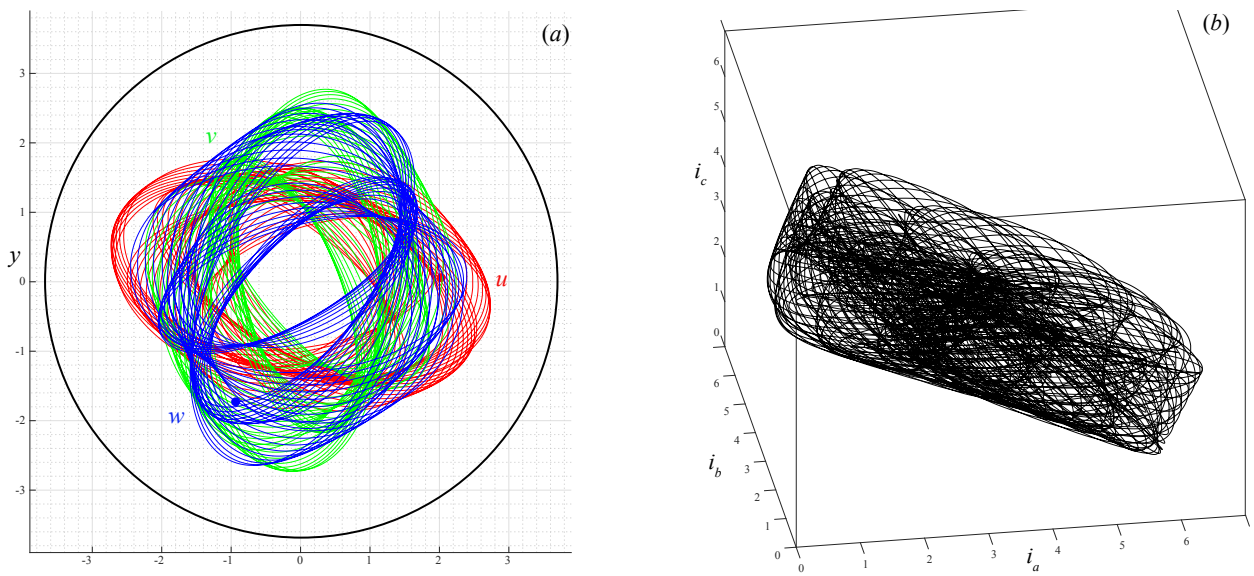

Figure 8. *A perturbed equilateral triangle. (a) Positions* (u, v, w) *in the plane as a function of time, up to* $t = 100$ *for* $U(P) = \frac{1}{2}P^2$*. Here the initial condition is an equilateral triangle with sides* $a = b = c = 2\sqrt{3}$*. (b) Trajectory in the positive octant of the inequities,* (i_a, i_b, i_c)*, for* $t = 200$*.. The initial conditions are* $u_0 = (2, 0)$*,* $v_0 = (-1, \sqrt{3})$ *and* $w_0 = (-1, -\sqrt{3})$*, with* $\dot{u}_0 = V_{rot}(0, 1) + \delta(\frac{1}{2}, -1)$*,* $\dot{v}_0 = \frac{1}{2}V_{rot}(-\sqrt{3}, 1)$ *and* $\dot{w}_0 = -\dot{u}_0 - \dot{v}_0$*. The perturbation is* $\delta = 3$ *and* $V_{rot} = 6$*. For this trajectory,* $E = 84.45577$*,* $J_T = 24.40192$*, and* $P_{max} = 11.2503$*, (5.2).*

followed by a several near collisions of u and v, and then a near collision of v and w at $t = 20.212$, where $a = 0.0440$. The evolution of the side lengths for this trajectory is shown in Fig. 11 for $t \in [0, 50]$. Of the many other near collisions, the closest, for $t \leq 500$, is $a(30.790) = 0.0004372$.

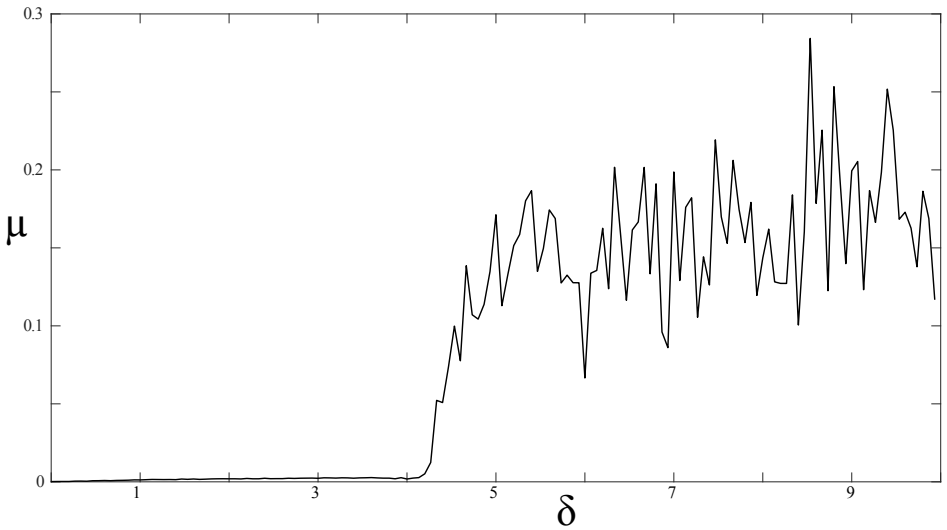

Figure 9. *The maximal Lyapunov exponent* μ_{2000} *for the equilateral initial condition of Fig. 8, with* $\dot{u}(0)$ *perturbed with* $\delta \in [0, 10]$*. The exponent appears to be zero up to* $\delta \approx 4.25$*.*

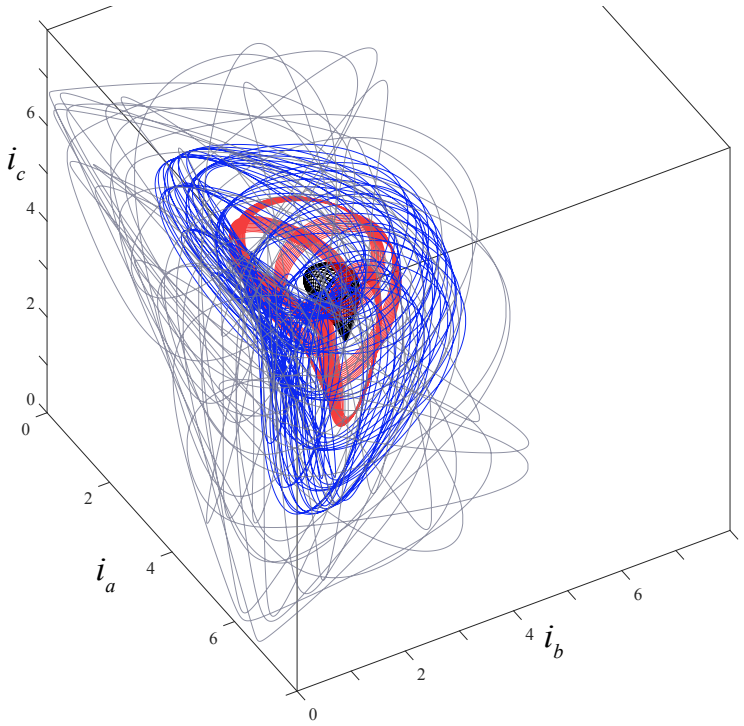

Figure 10. *Four trajectories in the space of inequities, up to $t = 50$ for the equilateral initial condition of Fig. 8, with $\delta = 0.5$ (black), 1.5 (red), 3.5 (blue), and 4.5 (gray). When $\delta = 0$, the orbit is an equilibrium in this space at $i_a = i_b = i_c = a = 2\sqrt{3}$. but is a uniformly rotating equilateral triangle in $\mathbb{R}^2$. The outermost orbit is chaotic since $\mu \approx 0.078 > 0$.*

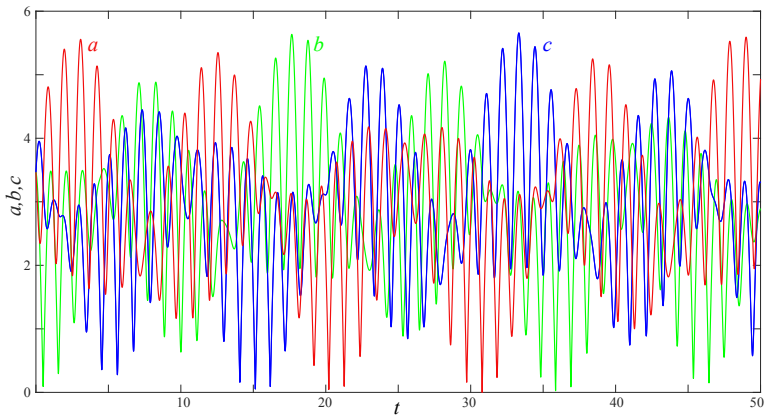

Figure 11. *The evolution of the triangle sides lengths a, b, c for the initial condition of Fig. 8 with $\delta = 4.5$. This trajectory was shown as the gray curve in Fig. 10. Note that there is a sequence of near pair-collisions, when a side length nears zero.*

Similar results are obtained for trajectories near the linear case discussed in §3.3. Here we

consider the set of initial conditions

$$
\begin{aligned}
&u(0) = (-2.5, 0), && v(0) = (0, 0), && w(0) = (2.5, 0),\\
&\dot{u}(0) = (1.5, -10.0711), && \dot{v}(0) = -\delta(0.5, 1.0), && \dot{w}(0) = -\dot{u}(0) - \dot{v}(0),
\end{aligned} \tag{5.3}
$$

for $\delta \in (0, 10]$. Most orbits in this family appear to have positive Lyapunov exponents, with values $0.006 \le \mu_{2000} \le 0.25$.

Finally, we consider an example of a trajectory for the areal case of §3.2, using the potential

$$U(\|A\|) = \frac{2}{\|A\|} + \|A\|^2 \ . \tag{5.4}$$

Since $U \to +\infty$ at $\|A\| = 0$ orbits cannot collapse to a linear configuration. For Fig. 12, the initial condition is equilateral, but the initial velocities do not have the symmetry (3.7). During the early evolution, seen in Fig. 12(a), $v(t)$ (green curve) remains relatively small, while the other two particles experience larger displacements. As seen in the inequity plot, Fig. 12(b), this orbit repeatedly passes close to the equilateral configuration, but then undergoes large swings towards either $i_c = 0$ or $i_b = 0$ where the triangle nears collapse to a linear configuration. For the areal case, the side lengths can become much larger than the perimetric case: indeed if the area were to approach zero, the perimeter could be unbounded. Of course, this is forbidden by the singularity in the potential (5.4); indeed for this energy, $U(\|A\|) \le E$ restricts the area to the range

$$0.3722962812 \le A(t) \le 2.139086602 \ . \tag{5.5}$$

The area and perimeter for $t \in [0, 500]$ are shown in Fig. 13; here $A(t) \in [0.37265, 2.13785]$, within 0.1% of the limits (5.5). The area undergoes much more rapid oscillations than the perimeter, which has the range $P(t) \in [3.68511, 81.24522]$. The corresponding moment of inertia (not shown) ranges over $I(t) \in [1.52569, 830.259]$. This again obeys the bound $I_{min} \ge P_{min}^2/9 = 1.50889$.

6. Conclusions. This paper has initiated the study of a rich new class of Hamiltonian systems: particles interacting in triplets with central forces. Geometrically such dynamics is interesting because the forces depend upon the shape of the triangle. Analytically, it is unconventional since physical models most often involve pair interactions. Nevertheless, as we noted in §2, triplet interactions also arise a number of physical systems. However, in most of these cases the three-body force is added to a more conventional two-body force. In our examples, we assumed there were only three-body forces.

In §3 we obtained the equations when the potential depends on the perimeter or area of the triangle. Perimetric potentials also occur in some applications; for example, such a potential for colloids was seen in (2.3). Potentials that obey the hypothesis of "centrality", Hyp. 2, could depend more generally on the side lengths, but if we ask that they are symmetric, Hyp. 3, a dependence on the perimeter or area seems natural. We are not aware of applications in which the potential has the areal form, though such forces have been studied in the context of gradient dynamics on hypergraphs as we noted in §2. In §5 we obtained numerical solutions for two simple examples, but in other explorations, we found that the dynamics has similar behavior for other potentials. The areal case has a weak singularity if the configuration passes through linearity, where the area is zero; moreover—as in the gravitational case—the triplet force can be singular when pairs or triplets coalesce. We have leave the study of such singularities to a future paper.

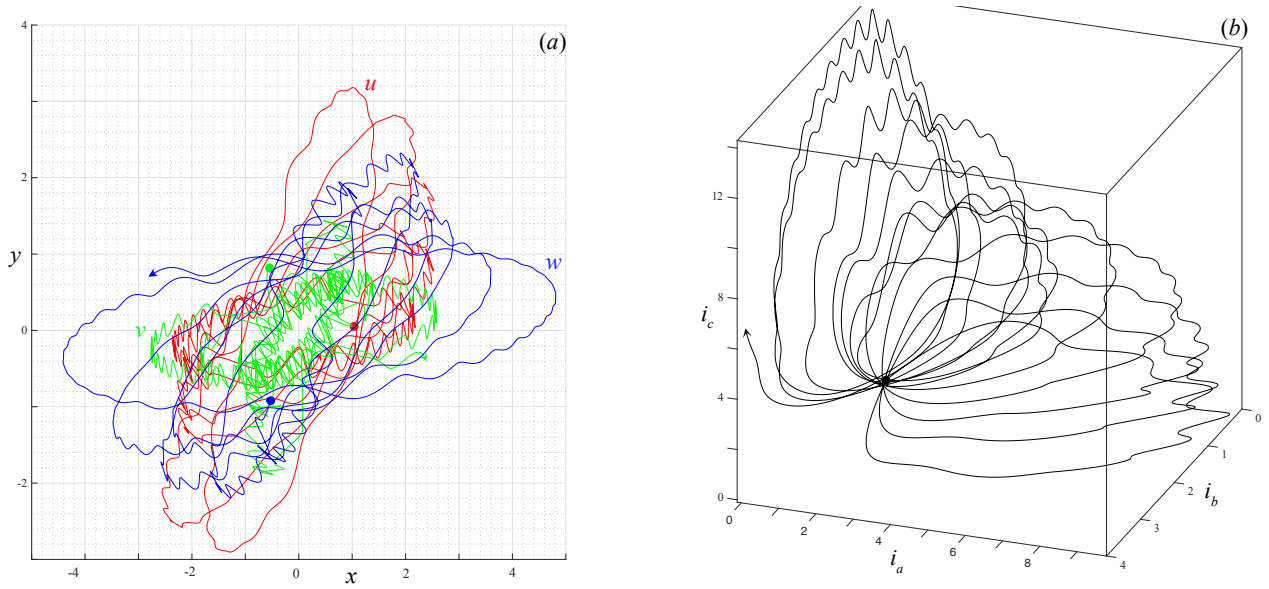

Figure 12. *(a) Positions of the three particles (u, v, w) in the plane as a function of time, up to $t = 100$ for the areal potential (5.4). (b) Trajectory in the positive octant of the inequities, (i_a, i_b, i_c). At $t = 0$, the triangle is equilateral with sides $a = b = c = \sqrt{3}$, setting $u_0 = (1, 0)$, $v_0 = \frac{1}{2}(-1, \sqrt{3})$, and $w_0 = \frac{1}{2}(-1, -\sqrt{3})$. The initial velocities are $\dot{u} = -\dot{w} = (1, 3)$ and $\dot{v} = 0$. For this trajectory, $E = 5.51067$ and $J_T = 1.99322$.*

We have found several special solutions: rotating equilateral triangle and linear configurations, and a non-rotating isosceles case. Many trajectories near the equilateral case lie on invariant tori, but they can become chaotic as the initial conditions vary—a typical phenomenon in Hamiltonian systems near an elliptic equilibrium. It would be interesting to see if there are other uniformly rotating solutions that might be analogous to the Lagrange points or central configurations of the gravitational problem [Ham19]. For such a study the Jacobi coordinates and its extensions [LMAC98] will prove useful. While we obtained this reduction in §4, we used a simpler convenient set of reduced coordinates, the triangular inequities, for visualization. An advantage of the later coordinates is that they respect the symmetry of the triplet system.

There is much to do in the future. For example, it would be interesting to study the case when there are more than three particles, as well as to allow for two body forces. It would also be interesting to investigate in more detail the stability of special solutions and families of invariant tori that generically occur in Hamiltonian systems due to KAM theory [MH92].

Appendices

Appendix A. Triangle Relations.

Given a triangle with vertices $(u, v, w) \in \mathbb{R}^9$, we let $(a, b, c) \in \mathbb{R}^{3+}$ (1.4) denote the lengths of each of the opposite sides, recall Fig. 1. The altitude of the triangle from the side c to w has length

$$h_c = a \sin(\theta_v) = b \sin(\theta_u) \; ; \tag{A.1}$$

where θ_u and θ_v are the interior angles at u and v respectively. This can be made more explicit by eliminating the sine functions. Define the signed distance between v and the base point of the

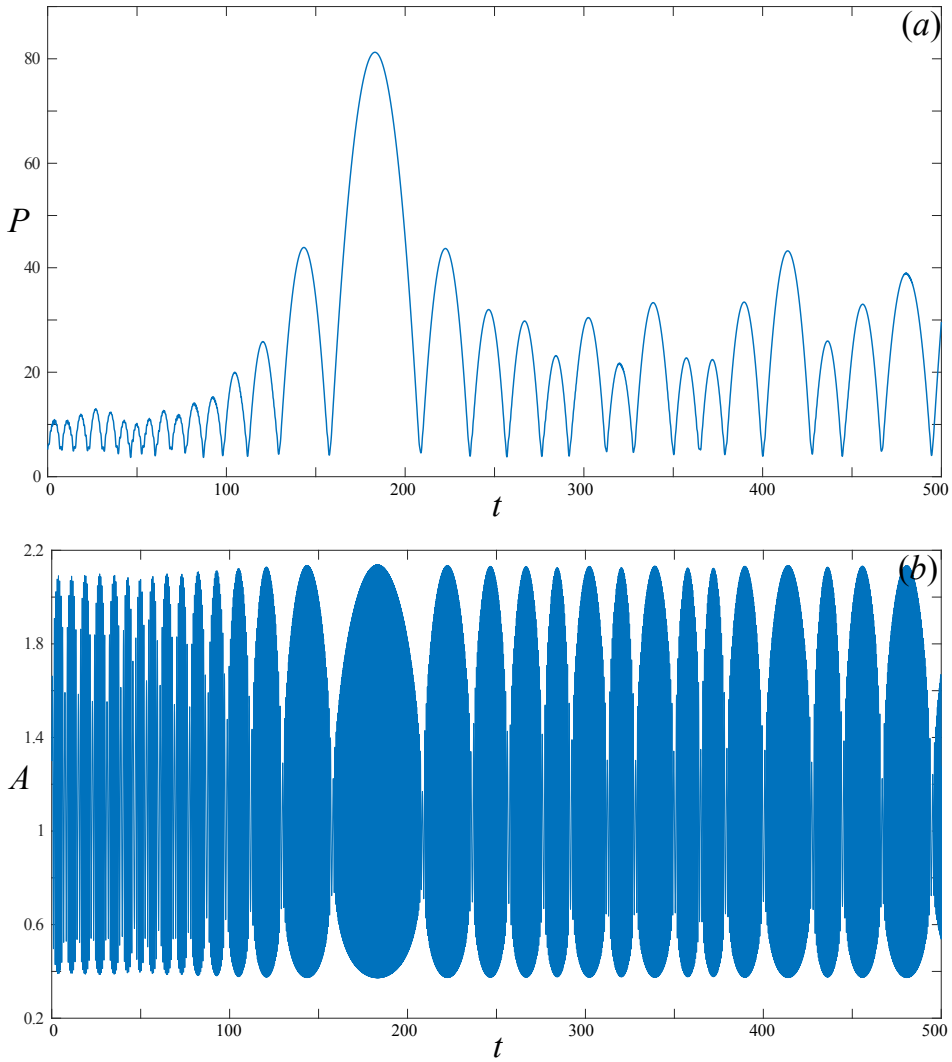

Figure 13. *For the potential (5.4) and the initial condition of Fig. 12, the perimeter (a) and area (b) as a function of time for* $t \in [0, 500]$.

altitude h_c by $x_c = a\cos(\theta_v) = c - b\cos(\theta_u)$, recall Fig. 1. Squaring (A.1) then gives

$$a^2(1-\cos^2(\theta_v)) = b^2(1-\cos^2(\theta_u)) \quad \Rightarrow \quad c^2 + a^2 - b^2 = 2cx_c \,. \tag{A.2}$$

With permutations, this gives the cosines of the interior angles:

$$\begin{aligned} \cos(\theta_u) &= \frac{b^2 + c^2 - a^2}{2bc} \,, \\ \cos(\theta_v) &= \frac{c^2 + a^2 - b^2}{2ca} \,, \\ \cos(\theta_w) &= \frac{a^2 + b^2 - c^2}{2ab} \,. \end{aligned} \tag{A.3}$$

By the triangle inequalities, the right hand sides of these formulas are indeed in the interval $[-1, 1]$.

By elementary trigonometry the magnitude of the area (3.4) is

$$\|A(u,v,w)\| = \tfrac{1}{2}ac\sin(\theta_v) = \tfrac{1}{2}ch_c \ .$$

We can solve for the altitude using $h_c^2 = a^2 - x_c^2$ and (A.2) to obtain

$$h_c = \frac{1}{2c}\sqrt{(a+b+c)(b+c-a)(c+a-b)(a+b-c)} \ .$$

This can be used with (A.1) to give formulas for the sines. Using this in the area gives Heron's formula

$$\|A\| = \tfrac{1}{4}\sqrt{(a+b+c)(b+c-a)(c+a-b)(a+b-c)} \ . \tag{A.4}$$

Note that (A.4) implies that the area depends only on the lengths of the sides, and, of course, is permutation symmetric.

The momenta of inertia, for the equal mass case is

$$I = \|u\|^2 + \|v\|^2 + \|w\|^2 \ .$$

Suppose that the coordinates are chosen so that the center-of-mass is at the origin, $R = \frac{1}{3}(u+v+w) = 0$, then after some algebra we can see that

$$I = \tfrac{1}{3}(a^2+b^2+c^2) \ .$$

More generally when the masses are not equal, this becomes (1.12). For a given perimeter $P = a+b+c$, this implies that $I \geq P^2/9$, with the bound occurring for the equilateral case.

Appendix B. Triangle Inequities. For a triangle with sides (1.4), the triangle inequality implies that $|a-b| \leq c \leq a+b$. We can use this, and its permutations, to define three nonnegative quantities that we will call the *inequities* of the triangle:

$$\begin{aligned} i_a &\equiv b+c-a \ , \\ i_b &\equiv c+a-b \ , \\ i_c &\equiv a+b-c \ . \end{aligned} \tag{B.1}$$

In terms of the inequities, the space of all possible triangles is the positive octant $(i_a, i_b, i_c) \in \mathbb{R}^{3+}$. Note that the inequities determine the sides:

$$a = \tfrac{1}{2}(i_b+i_c), \quad b = \tfrac{1}{2}(i_c+i_a), \quad c = \tfrac{1}{2}(i_a+i_b) \ ;$$

thus they uniquely determine the *shape* of the triangle. The perimeter (3.1) and area (A.4) become

$$P = i_a + i_b + i_c, \quad \|A\| = \tfrac{1}{4}\sqrt{P i_a i_b i_c} \ . \tag{B.2}$$

Surfaces of constant perimeter and area in inequity space are sketched in Fig. 14.

Each of the planes where one inequity vanishes corresponds to a degenerate triangle:

$$\begin{aligned} \{i_a = 0\} \simeq \{a = b+c\} &\Rightarrow \text{ Line with } u \text{ between } v \text{ and } w \ , \\ \{i_b = 0\} \simeq \{b = c+a\} &\Rightarrow \text{ Line with } v \text{ between } w \text{ and } u \ , \\ \{i_c = 0\} \simeq \{c = a+b\} &\Rightarrow \text{ Line with } w \text{ between } v \text{ and } u \ . \end{aligned}$$

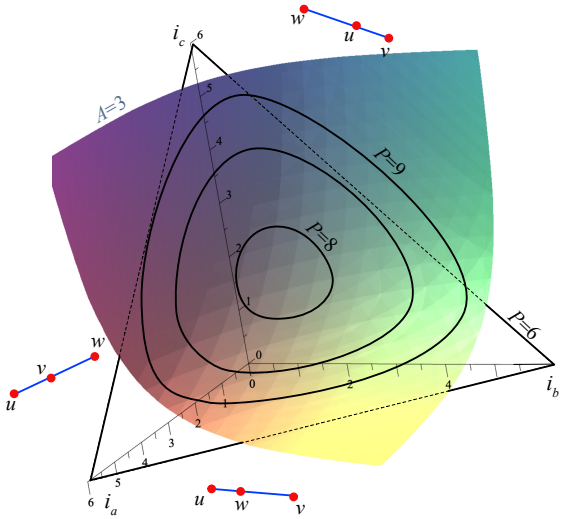

Figure 14. *Shape space of triangles in terms of the inequities (B.1). A surface of constant area, $A = 3$, is shaded. A partially dashed triangle outlines the plane where $P = 6$; this plane does not intersect the $A = 3$ surface, since (B.3) requires $P \gtrsim 7.8964$. Curves on the $A = 3$ surface with perimeters $P = 8, 8.5$, and 9 are also shown. Degenerate triangles are indicated on the coordinate planes.*

Examples are shown in Fig. 14. Thus the axes correspond to pair collisions,

$$\begin{aligned}
\{i_a = i_b = 0\} &\simeq \{c = 0\} \Rightarrow u = v \ , \\
\{i_b = i_c = 0\} &\simeq \{a = 0\} \Rightarrow v = w \ , \\
\{i_c = i_a = 0\} &\simeq \{b = 0\} \Rightarrow w = u \ .
\end{aligned}$$

Isosceles triangles lie on planes:

$$\begin{aligned}
\{i_a = i_b\} &\simeq \{a = b\} \ , \\
\{i_b = i_c\} &\simeq \{b = c\} \ , \\
\{i_c = i_a\} &\simeq \{c = a\} \ ,
\end{aligned}$$

and equilateral triangles are on the diagonal $i_a = i_b = i_c$. By (B.2), the plane of constant perimeter intersects the surface of constant area only when

$$P^2 \geq 12\sqrt{3}\|A\| \ , \tag{B.3}$$

and the first intersection is on the diagonal where the triangle is equilateral.

Appendix C. Incenter. The *incenter*, c_i, of a triangle is the center of the inscribed circle defined by the triangle, recall Fig. 2. It is also the unique point at which bisectors of the three angles meet. For a triangle with vertices (u, v, w), the bisecting line from a vertex u is

$$l_u(t) = u + t\left(\frac{v-u}{\|v-u\|} + \frac{w-u}{\|w-u\|}\right), \ t \in \mathbb{R} \ ,$$

with cyclic permutations for the two other vertices. Solving for the intersection point $c_i = l_u(t_1) = l_v(t_2) = l_w(t_3)$ gives the incenter (3.3), where P is the perimeter (3.1).

The point c_i is also the center of the inscribed circle in the triangle: each pair of right triangles formed from the triangle edges and the force line is congruent, so the three orange edges in Fig. 2 have equal lengths. The radius of the incircle is $r_i = \|c_i - u\| \sin(\theta_u/2)$, which, using the trig formulas in App. A, becomes

$$r_i = 2\frac{\|A\|}{P} \,. \tag{C.1}$$

There are two cases in which the incenter is at the center-of-mass of the triplet. If the particles are not collinear, we require that the opposites sides be proportional to the particle masses:

$$\|u - v\| = \alpha m_w, \quad \|v - w\| = \alpha m_u, \quad \|w - u\| = \alpha m_v,$$

for then (3.3) gives

$$c_i \to \alpha \frac{m_w w + m_u u + m_v v}{\alpha(m_w + m_u + m_v)} = x_{cm} \,.$$

Thus for the equal mass case, this occurs with an equilateral triangle.

If the particles are collinear, then the perimeter is twice maximum interparticle distance. Supposing, e.g., that v is between u and w, then $P = 2\|w - u\| = 2b$. In this case the incenter is the position of the central particle $c_i = v$.

Appendix D. Orthocenter. The orthocenter, c_o of a triangle is the intersection of the altitudes of the triangle (u, v, w), as shown in Fig. 3. To see that these lines intersect, parallel translate each side to its opposite vertex, to construct a new triangle (μ, ν, ω), see Fig. 15. The claim is that (u, v, w) is the medial triangle of (μ, ν, ω): the original vertices are bisectors of the sides of the new triangle. Moreover the circumcenter of (μ, ν, ω) is at the position of the orthocenter of the original triangle.

Solving for the position gives

$$c_o = v + \frac{(u - v) \cdot (v - w)}{2\|A\|} \hat{A} \times (w - u) \,,$$

or any cyclic permutation.

Appendix E. One-Jet. To compute the Lyapunov exponent for the perimetric case we use the one-jet of the vector field (3.2):

$$\begin{aligned} \delta\dot{p}_u &= U''(P)\left(\frac{v-u}{c} + \frac{w-u}{b}\right)\delta P + U'(P)\left(S_\perp^{v-u}\frac{\delta v - \delta u}{c} + S_\perp^{w-u}\frac{\delta w - \delta u}{b}\right) \,, \\ \delta\dot{u} &= \frac{\delta p_u}{m_u} \,, \end{aligned} \tag{E.1}$$

where

$$\begin{aligned} \delta P &= \tfrac{1}{c}(u - v) \cdot (\delta u - \delta v) + \tfrac{1}{b}(u - w) \cdot (\delta u - \delta w) + \tfrac{1}{a}(v - w) \cdot (\delta v - \delta w) \,, \\ S_\perp^x &= I - \frac{xx^T}{\|x\|^2} \,, \end{aligned}$$

are the perimeter variation and the matrix projection orthogonal to a vector x.

Acknowledgments. Useful conversations with Nathan Duignan, Robert Easton, Richard Montgomery, and Juan Restrepo are gratefully acknowledged. Thanks to the referees for providing helpful comments.

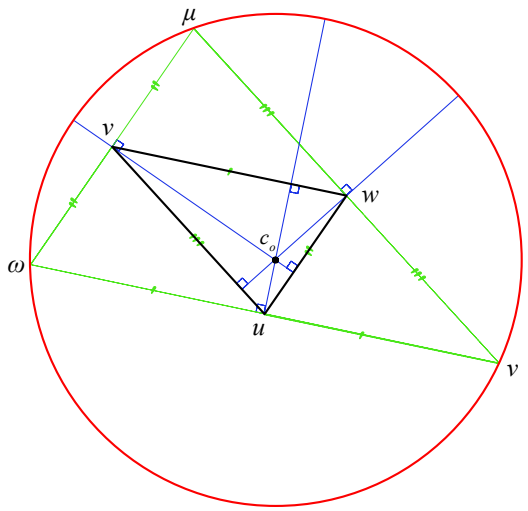

Figure 15. *Construction of the orthocenter of a triangle* (u, v, w)*. The sides of the triangle* (μ, ν, ω) *are parallel to each of the sides of the original triangle with the vertices* (u, v, w) *as bisectors. Thus the altitudes of* (u, v, w) *lie on the radii of the circumcircle of* (μ, ν, ω)*.*

REFERENCES

[AT43] B.M. Axilrod and E. Teller. Interaction of the van der Waals type between three atoms. *J. Chem. Phys.*, 11:299, 1943. https://doi.org/10.1063/1.1723844.

[Bas99] M. I. Baskes. Many-body effects in FCC metals: A Lennard-Jones embedded-atom potential. *Phys. Rev. Lett.*, 83(13):2592–2595, 1999. https://link.aps.org/doi/10.1103/PhysRevLett.83.2592.

[BMZ07] H. P. Büchler, A. Micheli, and P. Zoller. Three-body interactions with cold polar molecules. *Nature Physics*, 3(10):726–731, 2007. https://doi.org/10.1038/nphys678.

[CHLW97] C. Chakravarty, R.J. Hinde, D.M. Leitner, and D.J. Wales. Effects of three-body (Axilrod-Teller) forces on the classical and quantum behavior of rare-gas trimers. *Phys. Rev. E*, 56(1):363–377, 1997. https://doi.org/10.1103/PhysRevE.56.363.

[CPW83] J. Carlson, V. R. Pandharipande, and R. B. Wiringa. Three-nucleon interaction in 3-, 4- and ∞-body systems. *Nuclear Physics A*, 401(1):59–85, 1983. https://doi.org/10.1016/0375-9474(83)90336-6.

[DFB93] M.S. Daw, S.M. Foiles, and M.I. Baskes. The embedded-atom method: A review of theory and applications. *Materials Science Reports*, 9(7):251–310, 1993. https://doi.org/10.1016/0920-2307(93)90001-U.

[DKM+21] X. Dai, K. Kovalenko, M. Molodyk, Z. Wang, X. Li, D. Musatov, A. M. Raigorodskii, K. Alfaro-Bittner, G. D. Cooper, G. Bianconi, and S. Boccaletti. D-dimensional oscillators in simplicial structures: Odd and even dimensions display different synchronization scenarios. *Chaos, Solitons & Fractals*, 146:110888, 2021. https://doi.org/10.1016/j.chaos.2021.110888.

[FDGG24] T. Fukui, G. De Gregorio, and A. Gargano. Uncovering the mechanism of chiral three-nucleon force in driving spin-orbit splitting. *Phys. Lett. B*, 855:138839, 2024. https://www.sciencedirect.com/science/article/pii/S0370269324003976.

[Ham15] H.-W. Hammer. Three-body forces: From cold atoms to nuclei. *Acta Phys. Polonica B*, 46(3):379–390, 2015. https://doi.org/10.5506/APhysPolB.46.379.

[Ham19] M. Hampton. Planar n-body central configurations with a homogeneous potential. *Celestial Mechanics and Dynamical Astronomy*, 131(5):20, 2019. https://doi.org/10.1007/s10569-019-9898-0.

[Heb21] Kai Hebeler. Three-nucleon forces: Implementation and applications to atomic nuclei and dense matter. *Physics Reports*, 890:1–116, 2021. https://www.sciencedirect.com/science/article/pii/S0370157320303409.

[HW80] T. Halicioglu and P.J. White. Effect of three-body interactions on the structure of small clusters. *Journal of Vacuum Science and Technology*, 17(5):1213–1215, 1980. https://doi.org/10.1116/1.

570641.

[JTPW09] P. R. Johnson, E. Tiesinga, J. V. Porto, and C. J. Williams. Effective three-body interactions of neutral bosons in optical lattices. *New Journal of Physics*, 11(9):093022, 2009. https://dx.doi.org/10.1088/1367-2630/11/9/093022.

[KPS22] D. Kim, H. Park, and W. Shim. Higher-order interaction model from geometric measurements. Technical report, Simon Fraser University, 2022. http://arxiv.org/abs/2211.13001v1.

[Kö02] T. Köhler. Three-body problem in a dilute Bose-Einstein condensate. *Phys. Rev. Lett.*, 89(21):210404, 2002. https://doi.org/10.1103/PhysRevLett.89.210404.

[LMAC98] R.G. Littlejohn, K.A. Mitchell, V. Aquilanti, and S. Cavalli. Body frames and frame singularities for three-atom systems. *Phys. Rev. A*, 58(5):3705–3717, 1998. https://link.aps.org/doi/10.1103/PhysRevA.58.3705.

[Loh22] M.A. Lohe. Higher-order synchronization on the sphere. *Journal of Physics: Complexity*, 3:015003, 2022. https://doi.org/10.1088/2632-072X/ac42e1.

[LR97] R.G. Littlejohn and M. Reinsch. Gauge fields in the separation of rotations and internal motions in the n-body problem. *Rev. Mod. Phys.*, 69(1):213–276, 1997. https://doi.org/10.1103/RevModPhys.69.213.

[LR20] N.W. Landry and J.G. Restrepo. The effect of heterogeneity on hypergraph contagion models. chaos. *Chaos*, 30(10):103117, 2020. https://doi.org/10.1063/5.0020034.

[LS16] A. G. Lipnitskii and V. N. Saveliev. Development of n-body expansion interatomic potentials and its application for V. *Computational Materials Science*, 121:67–78, 2016. https://www.sciencedirect.com/science/article/pii/S0927025616301549.

[MH92] K.R. Meyer and G.R. Hall. *Introduction to the Theory of Hamiltonian Systems and the N-Body Problem*, volume 90 of *Appl. Math. Sci.* Springer-Verlag, New York, 1992.

[Mon17] R. Montgomery. The three-body problem and the shape sphere. *Amer. Math. Monthly*, 122(4):299–321, 2017. https://doi.org/10.4169/amer.math.monthly.122.04.299.

[Oks82] I. Oksuz. Effect of three-body forces on the structure of micro-clusters. *Surface Science*, 122(1):L585–L592, 1982. https://doi.org/10.1016/0039-6028(82)90053-X.

[RvGDvR02] C. Russ, H. H. von Grünberg, M. Dijkstra, and R. van Roij. Three-body forces between charged colloidal particles. *Phys. Rev. E*, 66(1):011402, 2002. https://doi.org/10.1103/PhysRevE.66.011402.

[SM25] E. Sander and J. D. Meiss. Computing Lyapunov exponents using weighted Birkhoff averages. *J. Phys. A*, 38:355701, 2025. https://doi.org/10.1088/1751-8121/adfac1.

[SS60] R.C. Smith and R.T. Sharp. Central three-body forces in heavy nuclei. *Canadian J. Phys.*, 39(9):1154–1167, 1960. https://doi.org/10.1139/p60-124.

[Sto13] A. Stone. *The Theory of Intermolecular Forces*. Oxford University Press, Oxford, 2013. https://doi.org/10.1093/acprof:oso/9780199672394.001.0001.

[Str00] S.H. Strogatz. From Kuramoto to Crawford: Exploring the onset of synchronization in populations of coupled oscillators. *Physica D*, 143(1-4):1–20, 2000. https://doi.org/10.1016/S0167-2789(00)00094-4.

[YE97] E. Yurtsever and N. Elmacı. Chaotic behavior of triatomic clusters. *Phys. Rev. A*, 55(1):538–544, 1997. https://doi.org/10.1103/PhysRevA.55.538.

[ZLB23] Y. Zhang, M. Lucas, and F. Battiston. Higher-order interactions shape collective dynamics differently in hypergraphs and simplicial complexes. *Nature Communications*, 14(1):1605, 2023. https://doi.org/10.1038/s41467-023-37190-9.